Finite Element Modelling of Machining of Metal Matrix Composites

Xiangyu Teng, Dehong Huo, and Islam Shyha

Abstract The fundamental material removal mechanism is central to understanding the machining process of metal matrix composites and improving such materials' machinability. Numerical models have been used extensively in the investigation of the machining process. It offers many advantages over experimental methods, particularly for examining the micro-scale phenomena that are hard to observe through experiments. This chapter will focus on the most widely used modelling method—finite element (FE) modelling. It starts from an overview of FE modelling on machining of MMCs. Then the general finite element model formulation is introduced. Finally, a case study using FE modelling on the cutting mechanism of Mg-MMCs reinforced with micro-sized and nano-sized particles.

1 Introduction

As one of the most common numerical simulation methods, the finite element (FE) modelling technique has been widely employed in the machining process studies to understand the material removal mechanism better. FE modelling can predict the cutting force, stress, strain, and temperature and chip formation during the cutting process. When compared to experimental research and other modelling techniques such as analytical modelling and molecular dynamics simulations, finite element method presents a better capability in predicting the behaviours of the material which is closer to reality: (1) tool-particles interaction, (2) particle fracture, (3) the merging of voids caused by debonding of particles, (4) surface generation during machining process [1]. As one of the most commonly used modelling methods, finite element modelling has gained increasing attention on studying the machining mechanism

X. Teng · D. Huo (✉)
Mechanical Engineering, School of Engineering, Newcastle University, Newcastle upon Tyne NE1 7RU, UK
e-mail: dehong.huo@newcastle.ac.uk

I. Shyha
School of Engineering and the Built Environment, Edinburgh Napier University, Edinburgh EH10 5DT, UK

I. Shyha and D. Huo (eds.), *Advances in Machining of Composite Materials*, Engineering Materials, https://doi.org/10.1007/978-3-030-71438-3_9

of MMCs in the past two decades. This chapter reviews the state-of-the-art in FE modelling of machining of MMCs, with emphasis on nano-MMCs. An overview of materials constitutive models, fracture criteria, and friction models is also presented. A case study on modelling of Mg-MMCs with SiC nanoparticles is given along with its micro-sized counterpart.

2 Review of FE Modelling on Machining of MMCs

Various numerical techniques have been used to model the machining process of MMCs in the past two decades. The modelling process can be achieved at two levels, namely in macro-mechanical and micro-mechanical models. Within macro-mechanical models, MMCs are treated as macroscopically anisotropic materials without considering fundamental characteristics such as particle size, interfaces between particles and matrix, and the fracture properties of particles. On the other hand, micro-mechanical models focus on the materials' local behaviour during the machining process. Thus they can predict the behaviour of particles such as debonding and fracturing during tool-particles interaction. Therefore it produces more visible details about the materials removal mechanism when compared to experimental approaches.

Different materials removal mechanism can be found in the machining of MMCs, which can be classified as follows: (1) the nucleation of voids due to debonding at the interface between particles and matrix, (2) particles failure. (3) growth and merging of voids in the matrix [1]. Those unique failure mechanisms in machining MMCs mean that their behaviour is different from that of homogeneous materials. According to numerous studies of finite element modelling on MMCs, it has been proven that various phenomena can be successfully simulated during the cutting process including particle failure, the flow of the particles in the tool-workpiece contact zone, debonding of the reinforcement in the secondary and primary deformation zones, and tool-workpiece interaction which leads to severe and premature tool wear.

The earliest attempt was conducted by establishing numerical investigation of the micromechanics involved during the machining of A356 aluminium alloy with 35% volume fraction of SiC particulate-based MMC using FORGE2 code [2, 3]. The whole simulation process was split into two stages. A homogeneous material was modelled to obtain the hydrostatic pressure in the first stage. The resultant loading output was applied in the second stage, accomplished using ANSYS, an elastoplastic FEA code. Using pressure data from aluminium alloy simulations, the particle–matrix interface failure, sub-surface damage, tool wear and residual stress were studied. Later, instead of simulating the two phases separately, a transient dynamics FE model was established to investigate the diamond turning process of Al6061/SiCp MMCs [4]. The normal and shear stresses field was studied in four different cases, namely tool facing/ploughing of aluminium matrix/SiC element respectively, and found that the relative position of the SiC element and cutting tool motion produced different

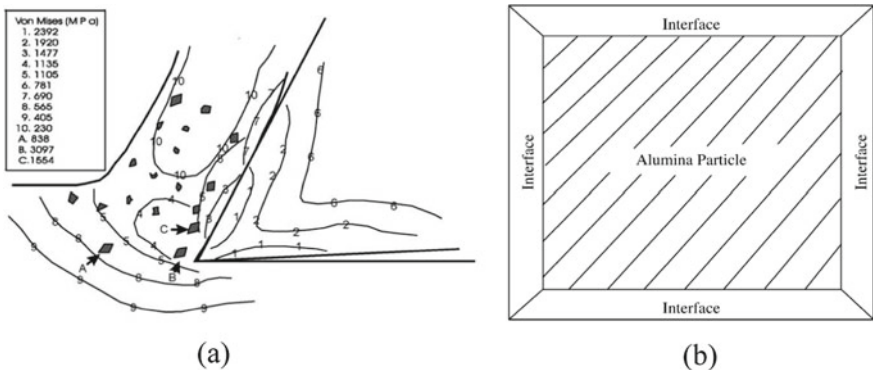

Fig. 1 **a** Von Mises stress distribution within matrix material; **b** modelling of particle interface. *Source* [5], with permission from Elsevier

magnitudes and patterns of stress. However, to better understand the material removal mechanism during machining, studying the interaction between the two phases is essential. Therefore, Zhu and Kishawy presented a plane-strain thermo-elastoplastic finite element model of orthogonal machining of Al6061/Al_2O_3 MMCs (Fig. 1) [5]. Temperature-dependent material properties were incorporated into this simulation. The effective and shear stresses on reinforcements and different machining deformation zones were investigated. The interface failure model between the matrix material and particles (e.g. particle debonding) was used to explain tool wear development. Although reinforcement was considered in this model, detailed cutting behaviours such as tool-particles interaction and particles' effect on the chip formation process were not simulated.

As the cutting tools pass through different phases of materials in the machining process, namely, soft matrix phase and hard. The abrasive nature of the reinforcement would cause the severe tool wear. This abrasive mechanism is hard to capture in machining experiment. Therefore, the interaction between particles and the cutting tool was studied through three scenarios with particles either above, along with or below the cutting path (Fig. 2) [4]. The variations in tensile and compressive stresses at the particles and the surrounding matrix as the tool advanced was investigated in these three scenarios and were used to explain the occurrence of particles fracture and to debond from the matrix. Additionally, the machined surface was considered hardened due to particles' indentation in the machined surface caused by interaction with the cutting tool. Apart from the excessive tool wear caused by machining MMCs, severer sub-surface damage compared with other machinable alloy is another challenge.

A multi-step 3D finite element model of sub-surface damage after the machining of MMCs was provided [6] (Fig. 3). The cutting data obtained from the initial step using an equivalent homogenous material (EHM) model was applied to a local multi-phase model. This multi-step method provided an accurate prediction of particle

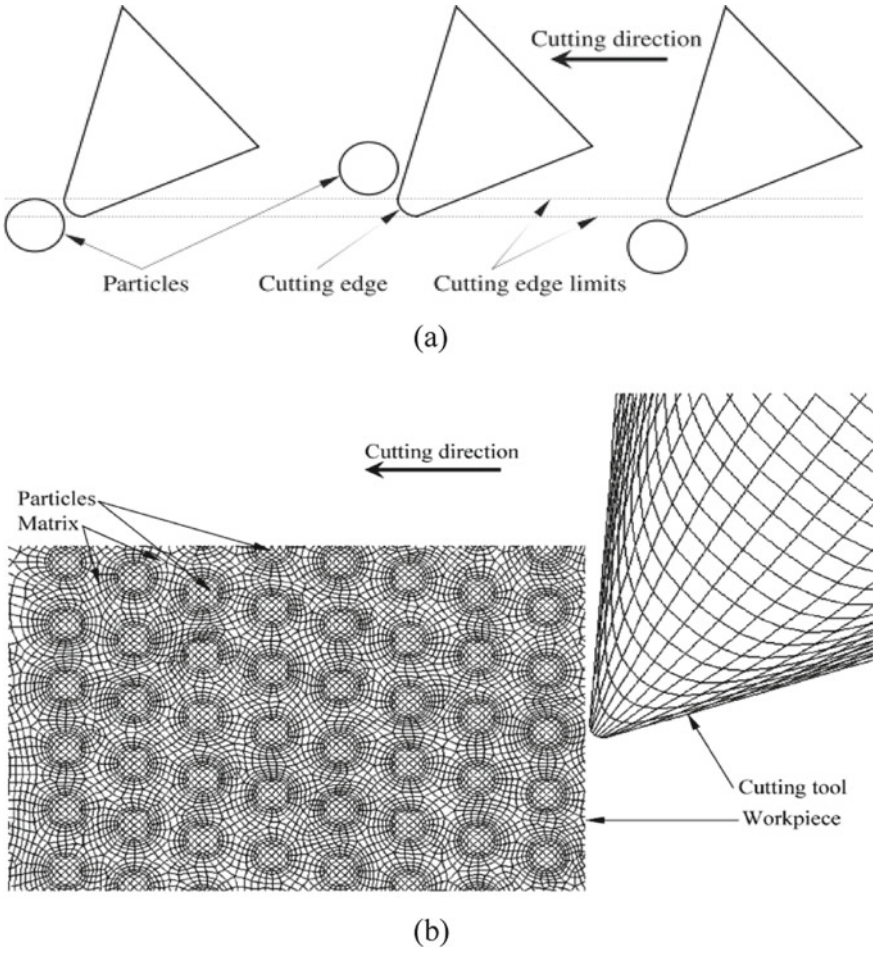

Fig. 2 **a** Three scenarios of tool-particles interaction; **b** Schematic representation for MMCs machining simulation. *Source* [4], with permission from Elsevier

fracture behaviour and the relationship between cutting force and depth of sub-surface damage.

Zhou et al. studied the removal mechanism by looking into the von Mises equivalent stress distributed locally within matrix and particle phases [7]. However, this simulation model exhibited an inability to globally simulate the chip formation process and stress/strain distribution under the particles' effect. To overcome this problem, the edge defects near the exit of orthogonal cutting by creating a FE model with randomly distributed particles was studied in later work [8]. The brittle fracture of particles and plastic flow of the matrix was found in the simulation process resulting in fragmented chips. The machined surface defects are also contributed

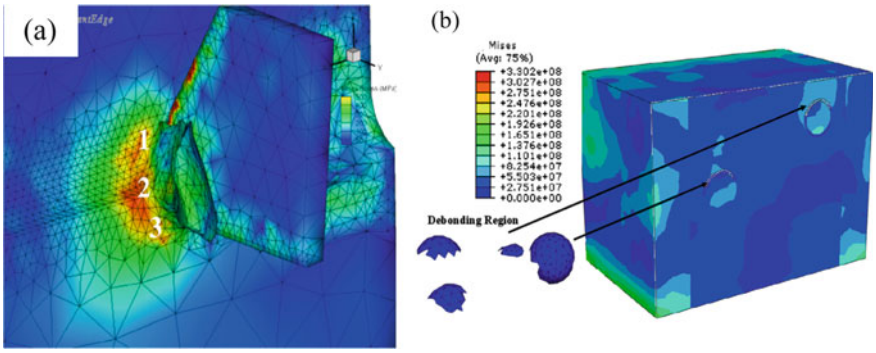

Fig. 3 **a** Stress distribution obtained from the machining EHM model; **b** sub-surface damage at a depth of 40.7 μm. *Source* [6], with permission from Elsevier

by particles failure behaviours such as debonding, microfracture, big cleavage, and cutting through particles [9].

Different model setting-up methods were attempted. A cohesive zone with predefined elastic modulus was added between the reinforcement and matrix phases [10]. The model with a cohesive zone element was more accurately predicted by cutting forces and chip morphology than the model without a cohesive zone. By introducing the cohesive zone, more local behaviours such as tool-particles interaction considering the effect of cutting speed by incorporating all phases of MMCs, including the matrix, particles and the interface between matrix and particles [11, 12]. Moreover, plastic deformation in the machining of Al6061/Al_2O_3 MMCs was analysed using the adaptive meshing technique to avoid mesh quality deterioration.

So far, most of the finite element modelling investigations have focused on machining MMCs with micro-sized particles. Only a few attempts have been made on machining of nano-MMCs. Teng et al. established a two-dimensional micromechanical finite element model to simulate the micro orthogonal machining of Mg-based MMCs reinforced with nanoparticles [13]. Unlike the fragmented chips obtained in machining MMCs with micro-sized particles, they found that continuously formed chips with a saw-tooth appearance were predominant. The reduction in particle size could induce significant changes in the material removal mechanism.

3 Overview of Finite Element Model Formulation

Several input factors for FEM such as the assignment of workpiece material properties (material constitutive model), criteria of chip separation (fracture criteria), friction within tool-chip interface, and mesh generation strategies are essential to provide a realistic model. The selection of appropriate factors critically affects the quality of output during the simulation. Among these factors, materials constitutive models, fracture criteria and friction models have been recognised as the three most important factors.

3.1 Materials Constitutive Model Formulation

An accurate material constitutive model is one of the most critical aspects to describe the behaviour of material deformation during the machining process. In reality, the workpiece material undergoes extreme conditions such as high strain, strain rate, and temperature increase. A high level of plasticity was observed in the primary and secondary shear zones. Meanwhile, a work hardening effect triggered by the fast strain rate of workpiece plays a vital role in determining its instantaneous mechanical properties, whilst the material properties measured in quasi-static conditions no longer govern the plastic behaviour. The material constitutive models used to describe stress and strain response and its dependence on strain and strain rate hardening and temperature softening effect have been proposed by researchers.

Among these material constitutive models, Johnson–Cook equation [14] has been widely used in FEM with adiabatic transient dynamic simulations. The factors affecting the workpiece's flow stress were classified into three terms: the elastic–plastic term representing the strain hardening. This viscosity presents increased flow stress with high strain rate and the temperature softening effect (Eq. 1).

$$\overline{\sigma} = \left[A + B\left(\overline{\varepsilon}^{pl}\right)^{n}\right]\left[1 + C\ln\left(\frac{\dot{\overline{\varepsilon}}^{pl}}{\dot{\varepsilon}_0}\right)\right]\left[1 - \left(\frac{T - T_{room}}{T_{melt} - T_{room}}\right)^{m}\right] \tag{1}$$

where $\overline{\sigma}$ is the flow stress, $\overline{\varepsilon}^{pl}$ is the plastic strain, $\dot{\overline{\varepsilon}}^{pl}$ is the plastic strain rate, $\dot{\varepsilon}_0$ is the reference strain rate, T is the workpiece temperature, T_{melt} and T_{room} are the material melting and ambient temperature. Coefficient A is the yield strength, B is the hardening modulus, C is strain rate sensitivity coefficient, n is the hardening coefficient, m is the thermal softening coefficient and these material coefficients are determined by experiments.

By considering the crystalline structure of a material, Zerilli and Armstrong [15] proposed a material constitutive model (Eqs. 2 and 3) based on the theory of dislocation mechanics. Two models based on the workpiece's lattice structure, including the body centre cubic (BCC) and face centre cubic (FCC), were established, as described respectively.

$$\overline{\sigma} = C_0 + C_1\exp\left[-C_3T + C_4T\ln\left(\dot{\overline{\varepsilon}}^{pl}\right)\right] + C_5\overline{\varepsilon}^{pl} \tag{2}$$

$$\overline{\sigma} = C_0 + C_2\overline{\varepsilon}^{pl}\exp\left[-C_3T + C_4T\ln\left(\dot{\overline{\varepsilon}}^{pl}\right)\right] \tag{3}$$

where $C_0 - C_5$ are materials constants determined through experiments. T is the absolute temperature.

The selection of material constants in constitutive models can critically affect outcomes such as stress and strain distribution, cutting force, temperature field, and chip morphology. Acquisition of these constants experimentally is a relatively

complex process since the experimental data is necessary to be acquired under the deformation conditions that cover an extensive range of strains, strain rate and temperature. Several constitutive models are also available to model the workpiece such as Mecking-Kocks [16] model with 23 material constants and a physical-based model with more necessary constants from 8 to 12 presented by Nemat-Nasser [17]. As J–C model and Z-A model require fewer constants than the two models mentioned earlier, they are widely used in material modelling studies.

3.2 Fracture Criterion

Materials separation is a complex process, including many physical mechanisms occurring at the micromechanical level [1]. Stress and strain were recognised as two main tensors that cause the initiation and evolution of materials fracture. In commercial FE software, the fracture mechanism can be classified into the ductile fracture and shear fracture. In ductile fracture, the voids would undergo the nucleation, growth and coalescence and eventually fracture. The mechanism in the shear fracture is mainly based on the shear band localisation. Recently, several fracture criteria for the ductile metal have been proposed and are widely used in various areas such as impact, fatigue analysis and metal forming process, which are (1) constant strain criterion and maximum shear stress criterion, (2) Johnson–Cook fracture criterion and (3) Cockcroft-Latham fracture criterion. Some of them are either built-in commercially available software or implanted through the user-defined subroutine.

3.2.1 Constant Strain Criterion

Constant strain criterion (Eq. 4) has been employed in many pieces of research regarding metal cutting and forming [5, 18, 19]. This criterion is assumed to be satisfied when the equivalent plastic strain reaches a critical value (equivalent strain at the onset of fracture). The workpiece's nodal point in front of the tooltip will be separated, resulting in the chips' separation. The disadvantage of this fracture criterion requires a high computational cost.

$$\omega_D = \int \frac{d\overline{\varepsilon^{pl}}}{\overline{\varepsilon_f^{pl}}} = 1 \tag{4}$$

where ω_D is a state variable.

The equivalent plastic strain at the onset of fracture is assumed to be a function of stress triviality and strain rate [20]:

$$\overline{\varepsilon}_f^{pl}\left(\eta, \dot{\overline{\varepsilon}}^{pl}\right) \tag{5}$$

where $\eta = -\mathrm{p/q}$ is the stress triaxiality, p is the pressure stress, q is the von Mises equivalent stress, $\dot{\overline{\varepsilon}}^{pl}$ is the equivalent strain rate.

3.2.2 Johnson–Cook Fracture Criterion

Johnson–Cook fracture criterion (Eq. 6) is a function of strain and strain rate hardening effect and temperature softening. It has been widely used to define the fracture criterion in metal machining. The equivalent plastic strain at the onset of fracture, $\overline{\varepsilon}_f^{pl}$, is defined as

$$\overline{\varepsilon}_f^{pl} = \left(d_1 + d_2 e^{d_3 \eta}\right)\left[1 + d_4 \ln\left(\frac{\dot{\overline{\varepsilon}}^{pl}}{\dot{\varepsilon}_0}\right)\right]\left[1 + d_5\left(\frac{T - T_{room}}{T_{melt} - T_{room}}\right)\right] \tag{6}$$

where $\mathrm{d_1} - \mathrm{d_5}$ are fracture parameter obtained from experiments, $\eta =$ is the stress triaxiality and $\dot{\varepsilon}_0$ is reference strain rate.

A damage parameter D is defined in each analysis increment, and the element would be deleted once damage parameter D reaches the unit value.

$$D = \sum \frac{\Delta \overline{\varepsilon^{pl}}}{\overline{\varepsilon_f^{pl}}} \tag{7}$$

Johnson–Cook simi-empirical fracture criterion and the constants can be determined through the tensile test, shear test or Hopkinson bar torsion with extensive strain rate and temperature [1].

3.2.3 Cockcroft-Latham Fracture Criterion

The Cockcroft-Latham fracture criterion was initially proposed for bulk forming operations (Eq. 8). However, a modified criterion was applied in machining simulation by numerous researchers [21–23]. The main disadvantage of this criterion is that it can be only used in small and negative triaxiality [1]. Same as other criteria as mentioned earlier, the onset of fracture initiates when the critical damage value, C, obtained through integration of the normalised maximum principal stress reaches the predefined value determined from the tensile test.

$$C = \int_0^{\varepsilon_f} \sigma^* d\overline{\varepsilon} \tag{8}$$

where $\sigma^* = \frac{\langle \sigma_1 \rangle}{\overline{\sigma}}$, the value of σ_1 is defined to be unity within this function if $\sigma_1 > 0$, and zero if $\sigma_1 < 0$, $\overline{\sigma}$ is equivalent stress.

3.2.4 Fracture Criterion Coupled with Damage Evolution Step

Generally, damage evolution step which is based on the accumulation of stress and strain can be used in combination with the fracture criteria aforementioned to model the progressive damage and failure of workpiece material. The materials failure process was divided into two steps, and the first step introduces the damage imitation while the second introduces the damage evolution. Two approaches can be employed to define the evolution process, including dissipated energy and effective plastic displacement.

Figure 4 presents the stress–strain response during the damage process. From point A to B, the material undergoes plastic strain with the hardening effect. Damage initiation is not satisfied at point B until the damage parameter D reaches unity, and σ_{y0} and $\overline{\varepsilon}_0^{pl}$ are the yield stress and equivalent plastic strain. After point B, the material undergoes the damage evolution process whilst the load-carrying capability is reduced until it reaches the failure state [20].

During the damage evolution process, the strain–stress response cannot illustrate the damage behaviour since it can cause a strong mesh-dependency based on strain localisation. Therefore, a fracture energy-based approach (Eq. 9) was proposed by Hillergorg [24]. The energy, G_f, was defined as a material parameter required to open a unit area of the crack. By utilising this approach, the mesh dependency is reduced, and the damage behaviour after the onset of fracture is decreased through a stress-displacement response.

$$G_f = \int_{\overline{\varepsilon}_0^{pl}}^{\overline{\varepsilon}_f^{pl}} L\sigma_y d\overline{\varepsilon}^{pl} = \int_0^{\overline{\mu}_f^{pl}} \sigma_y d\overline{\mu}^{pl} \tag{9}$$

where L is the characteristic length, $\overline{\mu}^{pl}$ is the equivalent plastic displacement.

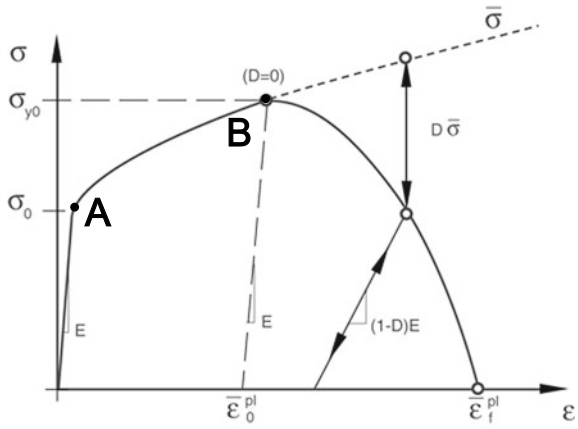

Fig. 4 Stress–strain curve of the damage evolution process

This approach introduces the equivalent plastic displacement, $\overline{\mu}^{pl}$ as the fracture work conjugate of the yield stress after the damage initiation point. The value of $\overline{\mu}^{pl}$ is defined as zero before the damage initiation and $\overline{\mu}^{pl} = L\overline{\varepsilon}^{pl}$ once the damage initiation criterion is satisfied.

For the damage evolution defined in terms of equivalent plastic displacement, a damage variable d (d = 0 at damage initiation point) was determined.

$$\mathrm{d} = \frac{L\overline{\varepsilon}^{pl}}{\overline{\mu}_f^{pl}} = \frac{\overline{\mu}^{pl}}{\overline{\mu}_f^{pl}} \tag{10}$$

Once damage variable d reaches unity, it can be thought that the load-carrying capability of a material is fully degraded, namely the failure of workpiece would occur. With the damage evolution defined in terms of energy, the equivalent plastic strain at failure can be expressed as:

$$\overline{\mu}_f^{pl} = \frac{2G_f}{\sigma_{y0}} \tag{11}$$

3.3 Friction Between Tool-Chip Interface

The friction characteristic at the tool-chip interface is one of the factors that significantly affect the simulated results. There are two shear zones taking place at the cutting tool's vicinity; primary shear zone due to the large strain and strain rate, secondary shear zone due to the friction at the tool-chip interface. The friction characteristic is very complicated. A large amount of heat can be generated due to friction at the tool-chip interface with high cutting speed leading to a high temperature field, which eventually facilitates the process of excessive tool wear. The simplest way is to experimentally acquire a constant coefficient of friction and apply it along with the tool-chip interface.

In most studies, Coulomb friction law combining with the sticking-sliding theory is applied to simulate friction stress. Two regions, including sticking and sliding, are established along with the tool-chip interface. A sticking region forms at the cutting tool's vicinity and the friction shear stress (Eq. 12) is equal to the average shear flow stress in the chips, k_{chip} [25]. Once the shear stress at interface reaches a critical value (limiting shear stress), sliding regime (Eq. 13) govern the friction process. Sliding region forms along the remainder region along with the interface and the friction shear stress can be determined using a coefficient of friction, μ.

$$\tau_{sticking} = k_{chip} \text{ when } \mu\sigma_n < \tau_{lim} \tag{12}$$

$$\tau_{sliding} = \mu\sigma_n \text{ when } \mu\sigma_n \geq \tau_{lim} \tag{13}$$

where τ_{lim} is the limiting shear stress, σ_n is normal stress distribution along the rake face, $\tau_{sticking}$ is friction shear stress along the sticking region, $\tau_{sliding}$ is friction shear stress along the sliding region, μ is the friction coefficient.

4 FE Modelling on the Cutting Mechanism of Nano-Particles MMCs

In this section, a comprehensive introduction on the study of finite element modelling of MMCs reinforced with nanoparticles conducted by Teng et al. [13] will be presented.

4.1 Modelling Procedures

The model is based on the micro-milling of Mg-MMCs reinforced with SiC nanoparticles. An assumption [26] has been made for simplifying 2D micro-milling process to orthogonal machining process. In micro milling experiment conducted within this study, the maximum uncut chip thickness t (less than 2 μm) is much smaller than the diameter of micro endmill (500 μm) as shown in Fig. 5a. It results in a relatively small variation of uncut chip thickness (2 μm) when compared with the travel distance of cutting edge in 180° of tool rotation (~392.5 μm), it can be thought that the variation of uncut chip thickness will not make a significant influence on results (e.g. cutting force and chip morphology). Therefore, the uncut chip thickness in the micro-milling process can be considered equivalent to that in the orthogonal machining process, as shown in Fig. 5b.

A two-dimensional micro-mechanical finite element model is established to simulate the micro-orthogonal machining process of nano Mg/SiC MMCs using commercially available software ABAQUS/Explicit v6.14–4. Since the nonlinearity, immense strain and strain rate are involved in the machining process, arbitrary Lagrangian–Eulerian (ALE) formulation is selected to avoid severe distortion of elements. The schematic representation of the established model is shown in Fig. 5. The cutting tool which moved horizontally into the workpiece with a predefined speed. To better understand the machining process details, two phases materials, including matrix and particles, are assigned individually in this model. The particle diameter is defined as 100 nm, with a volume fraction of 1.5%. The machining parameters are listed in Table 1.

A particles distribution strategy that makes the particles distributed at different relative locations of cutting path is used in this model, as shown in Fig. 6a. Within this strategy, the distance between each particle in X and Y direction is the same. In contrast, the distance between the uppermost particles and top surface of the workpiece is 50 nm larger in Y direction than the last column from right to the left

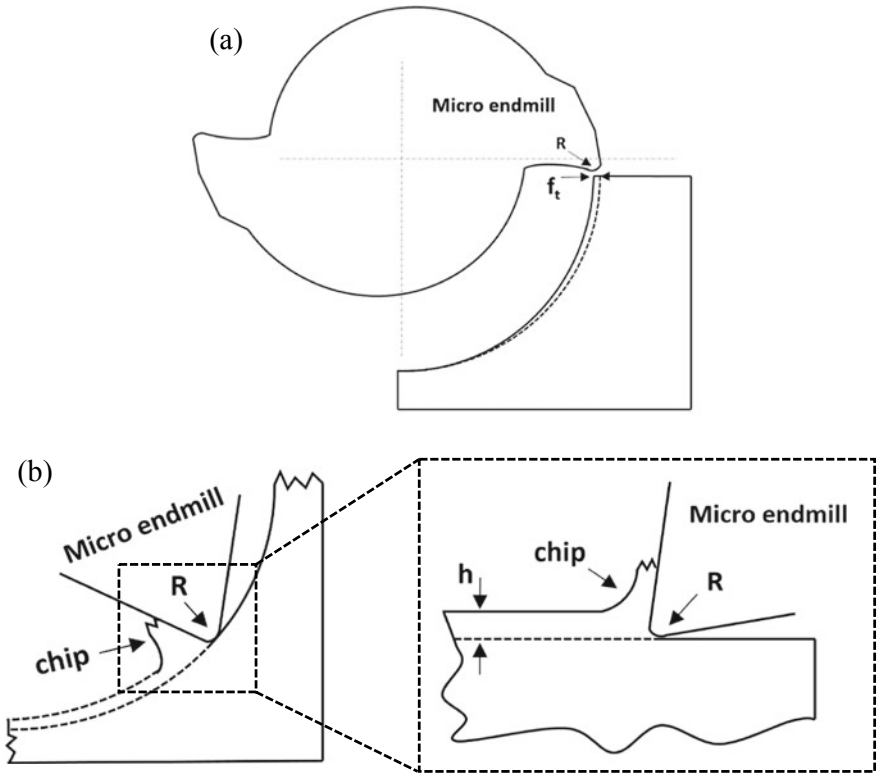

Fig. 5 **a** Schematic diagram of the 2D milling process in 180° of tool rotation; **b** Relationship between 2D milling process to the orthogonal machining process. *Source* [13], with permission from Elsevier

Table 1 Machining parameters in the FE model

Cutting speed, V_c (m/min)	125.64
Uncut chip thickness, t (μm)	0.1, 0.2, 0.5, 1, 2
Tool rake angle, α (Degree)	10
Tool clearance angle, β (degree)	6
Cutting edge radius, (μm)	1

side. For example, particles along line A distribute further away from bottom cutting edge limits, representing the diversity of particles locations relative to the cutting path in reality.

Magnesium matrix is treated as a deformable thermo-elastic–plastic material with quadrilateral continuum element and fracture criteria. Johnson–Cook constitutive model is used to describe the plasticity behaviour of magnesium matrix during the machining process. Johnson–Cook fracture equation is used to define the materials failure criterion for magnesium matrix. SiC particles were assumed to be a brittle

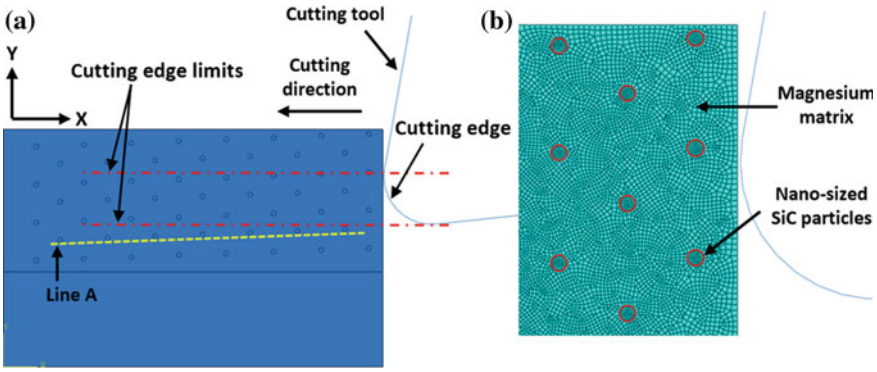

Fig. 6 **a** Schematic representation of the established models for micro orthogonal machining of Mg/SiC MMCs; **b** Local zooming of mesh element. *Source* [13], with permission from Elsevier

cracking body with brittle failure definition to investigate its behaviour during the cutting process. Free thermal-displacement quad-dominated meshing technique is used to advance the front algorithm for both matrix and particles. Mesh size of particles and matrix surrounding particles is defined to be 25 and 40 nm. The bottom surface of the models was fixed in all directions. The surface-to-surface contact model is applied between the external surface of the tool and node points of the machining area.

4.2 Chip Formation Process Analysis

Figure 7 illustrates the simulated chip formation process under the uncut chip thickness of 1 μm. As shown in Fig. 7a, when the tool firstly engages with the workpiece, highly concentrated stress is induced leading to an irregular shear zone closely formed in front of the cutting edge, which is different from that in macro machining of MMCs where an apparent primary shear zone can be formed at the initial cutting stage.

As the tool advances, the primary shear zone can be observed in Fig. 7b. Additionally, the particles take more stress than matrix material, especially those particles located near the primary shear zone. This is attributed to the high elasticity of SiC particles. The maximum von Mises stress is found at the particles located under cutting edge, 3109 MPa. This is different from machining monolithic materials where the maximum stress occurs in the primary shear zone.

Moreover, another difference can be obtained by observing the von Mises stress distribution pattern in Fig. 8. The addition of nanoparticles significantly alters the pattern of stress field within the matrix. A distorted stress contour can be found at the vicinity of each particle. This observation can be explained by particles' existence in the matrix, restricting the progression of plastic stress flow within the matrix during the machining process. The stress is accumulated and results in a high plastic strain

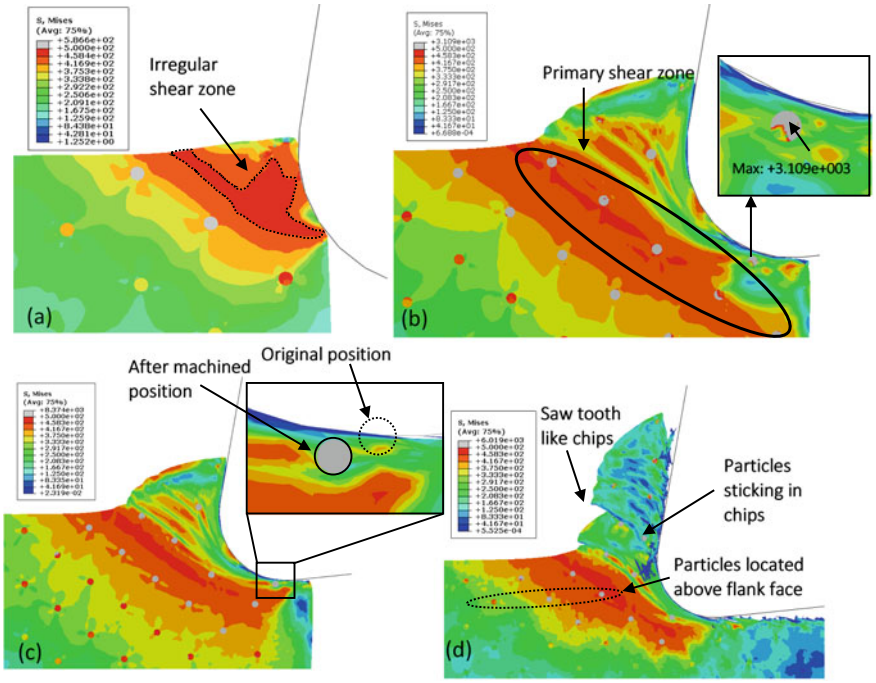

Fig. 7 Chip formation process during the micro-machining of nano Mg/SiC MMCs. *Source* [13], with permission from Elsevier

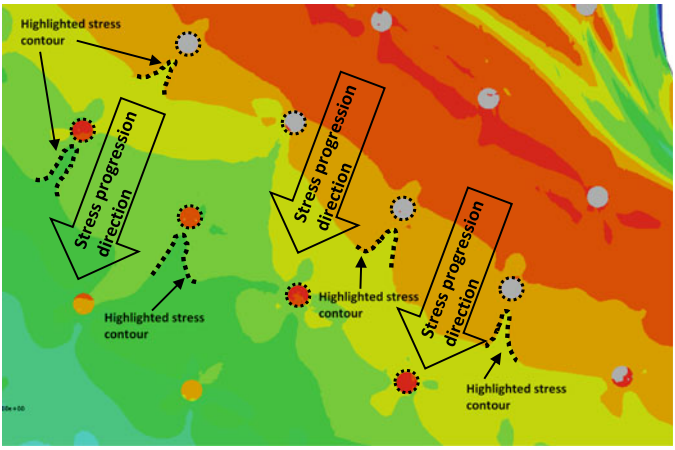

Fig. 8 Effect of addition of nanoparticles on the distribution pattern of von Mises stress contour. *Source* [13], with permission from Elsevier

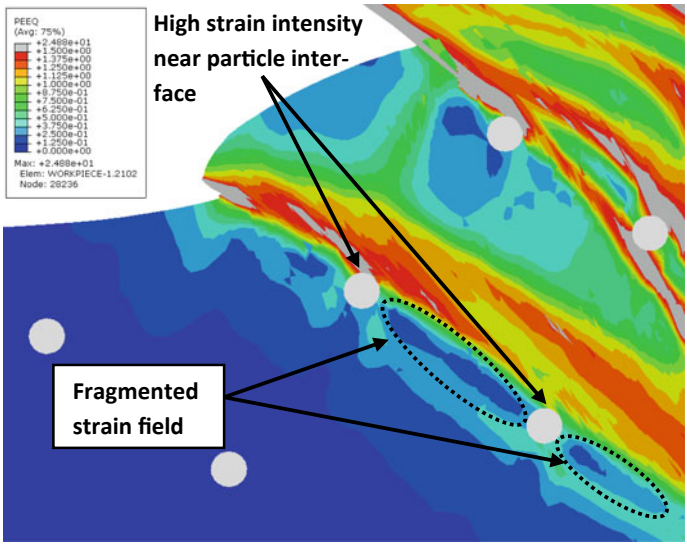

Fig. 9 Distribution of equivalent plastic strain within nano Mg/SiC MMCs. *Source* [13], with permission from Elsevier

field at particle interface, as shown in Fig. 9. The existence of nanoparticles also fragments strain field. Similar phenomena were reported by Pramanik et al. [5] in the machining of micro-sized Al/SiC MMCs.

As the tool continuously moves, Fig. 7c shows the behaviour of a particle located immediately under the flank face of the cutting tool when the tool is approaching it. Comparing with the original position of this particle moves horizontally with the highly deformed matrix in cutting direction without any direct contact with the cutting edge. Evolution of von Mises stress on the matrix element surrounding the particle with the cutting edge approach is studied in Fig. 10 in details. Initially, von Misses stress is found to increase to a maximum value of 454 MPa (C) with the tool's advancement. At this stage, the particle is found at primary shear zone. As mentioned earlier, this particle acting as a barrier restricts plastic stress progression within the matrix, which results in high compressive stress acting on the matrix close to the particle interface. This is different from the macro machining process. The maximum stress usually happens at the matrix between cutting edge and particles due to the indention caused by the cutting edge [4].

Consequently, this results in concentrated stress ranging from 540 to 650 MPa acting at particles. A sudden drop in von Mises stress is followed from C to E as the primary shear zone moves horizontally passing through this particle. At this period, the restricting behaviour on plastic stress flow of particle becomes less dominant as particles move with the surrounding matrix with further advancement of the tool. It is believed that the matrix element experiences a highly plastic deformation within this stress drop process (C to E). Finally, von Mises stress releases and decreases to

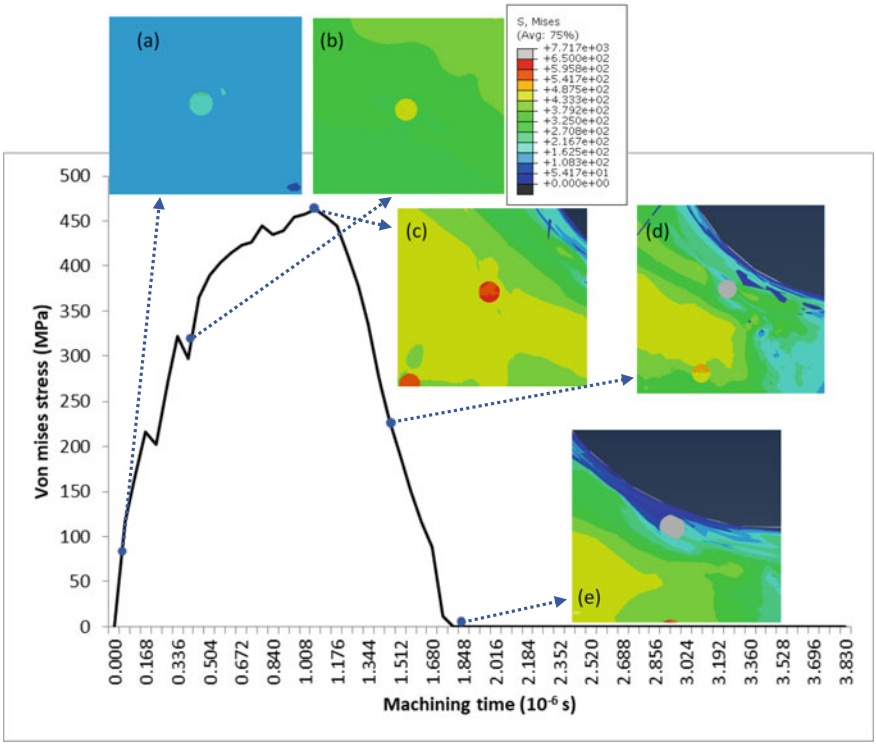

Fig. 10 Evolution of von Misses stress distribution on the matrix element close to the interface of particle. *Source* [13], with permission from Elsevier

0 MPa when the cutting edge passes through it, failing the matrix surrounding this particle. As a result, this particle is subjected to debonding from the matrix.

The premature tool wear caused by the high contact stress between the cutting tool and hard particles has been recognised as one of the crucial factors affecting the machinability of MMCs. The interaction process between the cutting tool and particles should be better analysed to predict the tool wear. Figure 11a–d illustrates the stress distribution on the particles located immediately below the cutting edge with the tool's advancement. Based on the observation of Fig. 11a and b, the increase in von Mises stress can be observed on the particle due to the compressing of the surrounded matrix with tool approaching the particle. The direct contact between tool and particles can be found in Fig. 11c. Highly concentrated stress on the particle's upper part is generated due to the ploughing between particle and flank face. This particle is then debonded and slide over the flank face (Fig. 11d). During the sliding process, particle acting as a sharp cutting edge scratches the flank face leading to abrasive wear. Smoother wear at the flank face is expected due to the nanoparticles. Additionally, it is evident from this figure that the particle is still intact, which is

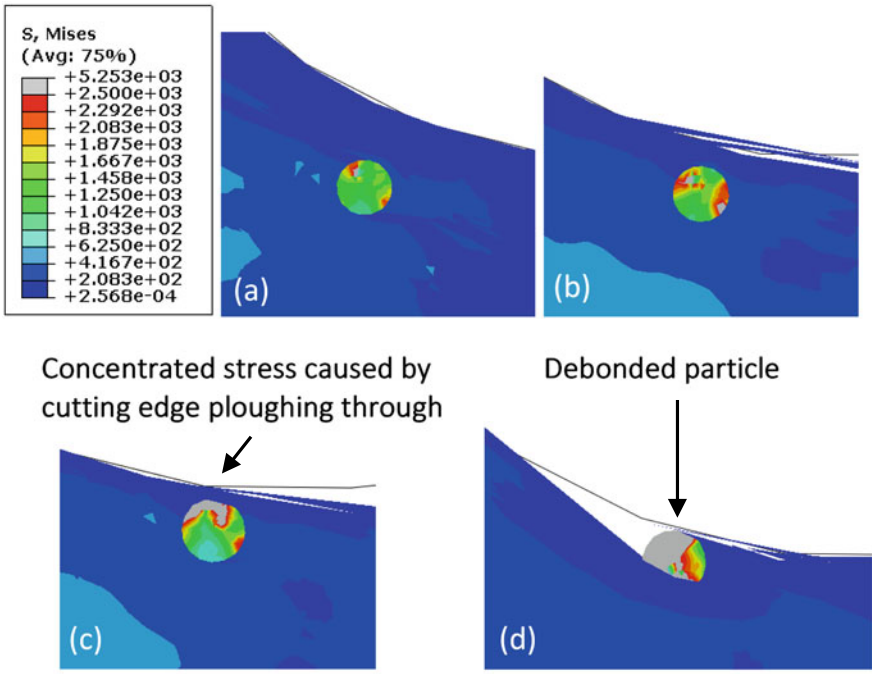

Fig. 11 Evolution of von Misses distribution on the particle located immediately below cutting edge with the cutting tool's advancement. *Source* [13], with permission from Elsevier

different from that in the machining of micro-sized MMCs where particle fracture is observed.

Upon the advancement of the cutting tool, the chip is completely formed (Fig. 7d). A complete chip-tool contact area is achieved with chip flow happening along the rake face. In this stage, the particles located above the cutting tool's flank face initially move with the surrounding matrix and enter into the formed chips as the cutting edge approaches. Figure 7d also illustrates a continuous chip with saw tooth appearance. This phenomenon can be explained by studying the equivalent plastic strain distributed in the chip. As shown in Fig. 12, a large deformation is observed at the chip and cutting tool interface.

Moreover, it can be seen that several highly strained bands are distributed across the chips at the vicinity of particles, which can be considered as the main reason contributing to the lamellate structure of chips. Those highly strained bands are mainly caused by localised high plastic von Mises stress bands (Fig. 13). Figure 13 illustrates the formation of high-stress bands within chip with the advancement of the cutting tool. At the initial stage, the primary shear zone is observed in Fig. 13a. As the tool further moves, the transition stage is achieved (Fig. 13b). The concentrated stress field is observed at the particles' interface as the primary shear zone passing

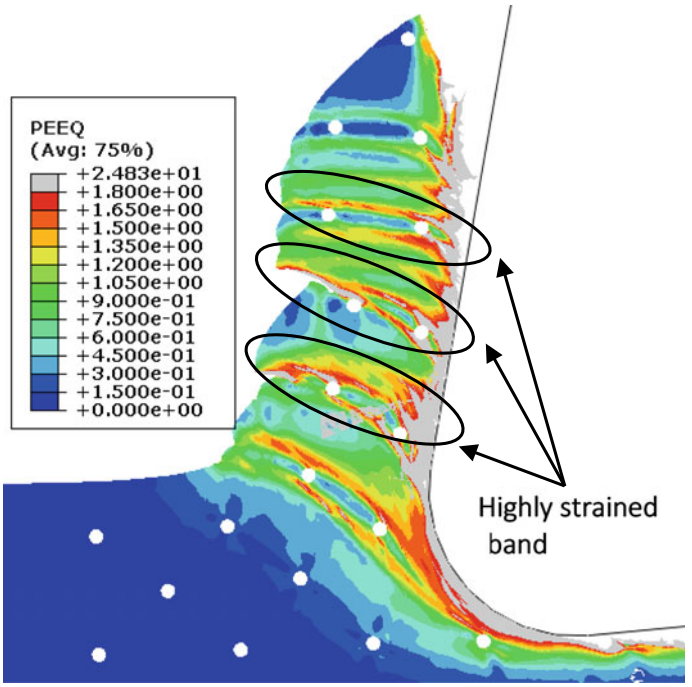

Fig. 12 Distribution of equivalent plastic strain within formed chips. *Source* [13], with permission from Elsevier

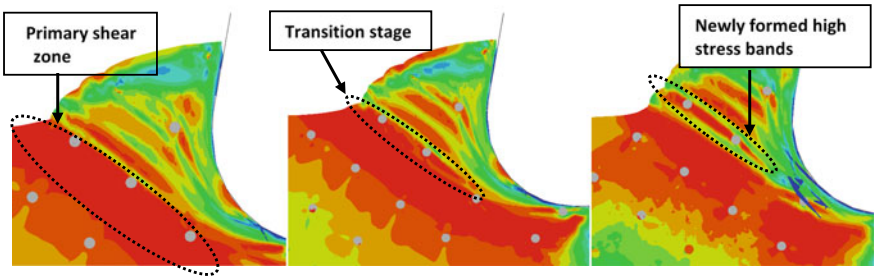

Fig. 13 Formation of high-stress bands within chips with the advancement of the cutting tool. *Source* [13], with permission from Elsevier

through due to particles' restricting behaviour to plastic stress flow, as mentioned earlier. Figure 13c shows that eventually, the high-stress bands is formed within chips.

4.3 *Effect of Uncut Chip Thickness*

Specific cutting force can be calculated by dividing the resultant cutting force by the section area of the cutting area. Figure 14 shows the specific cutting force at different uncut chip thickness obtained from the machining experiment and simulation model. A sudden decrease can be observed when the uncut chip thickness is less than 0.5 μm. Then the specific cutting force decreases mildly with the increase of uncut chip thickness.

Several differences will appear when the machining features decrease from macro to micro-scale. One of the significant concerns is the size effect leading a transitional regime associated with intermittent shearing and ploughing in the material removal process [27]. In this section, the chip morphology of micromachining on nano Mg/SiC MMCs under various uncut chip thickness is investigated through FE models (Fig. 15). Minimum chip thickness is determined based on the studying of chip morphology. The uncut chip thickness is selected to be 0.1, 0.2, 0.5, 1 and 2 μm. As shown in Fig. 15, the highly concentrated stress region can be considered the primary shear zone observed within workpiece materials with different locations underneath the cutting edge at all uncut chip thickness.

At uncut chip thickness of 0.1 μm, it can be found from Fig. 16 that there is no continuous chip formed in the cutting process. The small amount of material is initially elastically 'pushed' and accumulated in front of cutting edge (Fig. 16a). With the tool continuously moving, the equivalent strain at the chip root increases, resulting in plastic deformation. Figure 16c illustrates the continuous cutting stage. The maximum equivalent plastic strain is distributed at the accumulated material, which finally leads to a complete failure and stress within workpiece is released. The fragmented chip is therefore formed by this discontinuous removal mechanisms. The chip formation process at an uncut chip thickness of 0.2 μm exhibits a similar behaviour like that of an uncut chip thickness of 0.1 μm. When the uncut chip

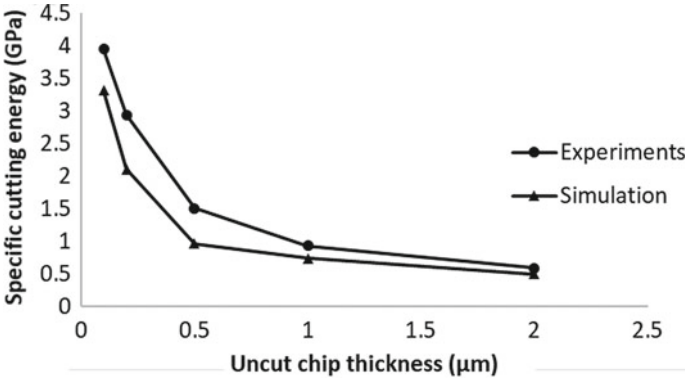

Fig. 14 Specific cutting force at different uncut chip thickness. *Source* [13], with permission from Elsevier

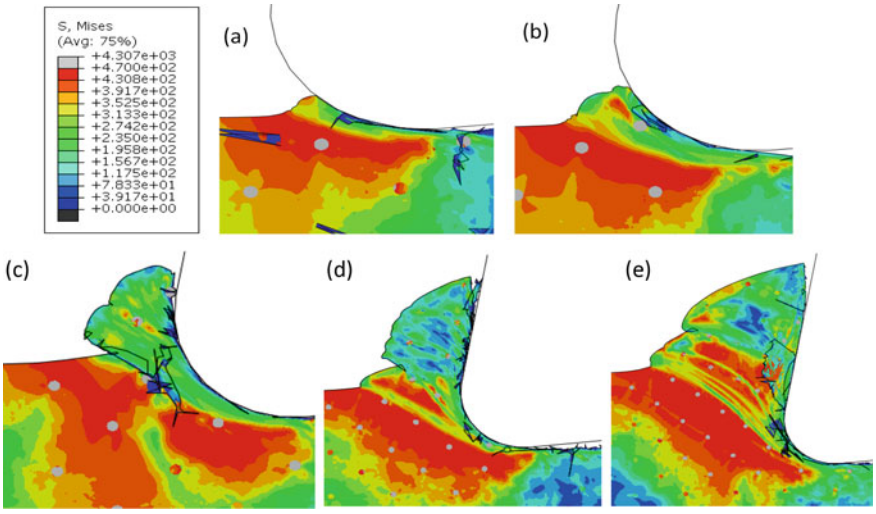

Fig. 15 Chip morphology at uncut chip thickness of **a** 0.1 μm; **b** 0.2 μm; **c** 0.5 μm; **d** 1 μm; and **e** 2 μm. *Source* [13], with permission from Elsevier

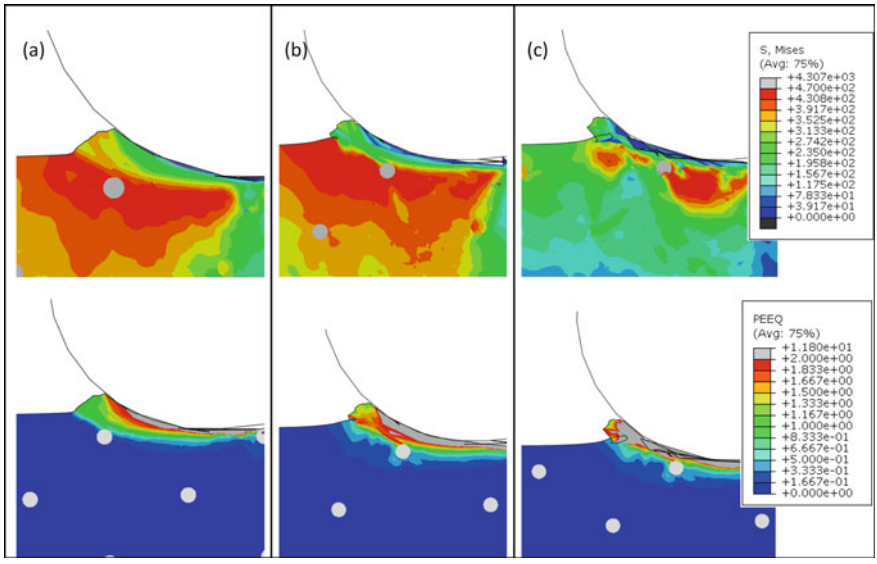

Fig. 16 Stress and strain distribution within workpiece at material removal process under the uncut chip thickness of 0.1 μm. *Source* [13], with permission from Elsevier

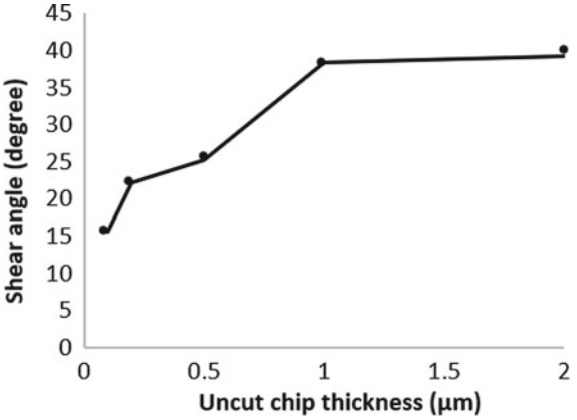

Fig. 17 The variation of shear angle with uncut chip thickness in the FE model. *Source* [13], with permission from Elsevier

thickness increase to 0.5 to 2 µm, an irregular segmented chip is formed. Based on these results, the minimum chip thickness can be proposed to be 0.5 µm (0.5R) under the input parameters utilised in this FE model. This result is consistent with that obtained from research carried by Teng et al. [28], which is 0.53R in micromachining of Mg/Ti with a volume fraction of 1.98%. Moreover, an increase in the shear angle can be found with the uncut chip thickness (Fig. 17).

5 Comparison Between Micro-Sized and Nano-Sized Particles Reinforced MMCs

In this section, simulation models machining of two types of MMCs reinforced with micro-sized particles and nanoparticles were developed respectively. This section presents a comparison between machining of micro and nano-MMCs in terms of chip formation, stress/strain distribution, tool-particles interaction and machined surface morphology. Finally, validation of FE models is conducted by investigating tool wear, chip morphology and machined surface morphology obtained from micro-milling experiments.

5.1 Von-Mises Stress Distribution in the Cutting Area

Chip formation process accompanying with the stress distribution when micromachining of Al/SiC MMCs reinforced with nano-sized and micro-sized particles were illustrated in Figs. 18 and 19, respectively. Figures 18a and 19a show the initial contact stage between the deformed workpiece and cutting tool before chip formation. Particles distributing at the matrix experiencing with highly concentrated stress

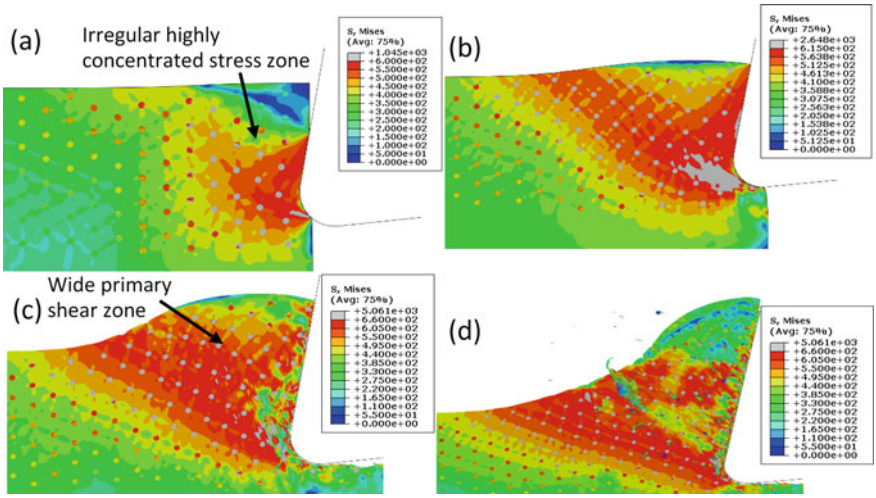

Fig. 18 Chip formation when micromachining of Al/SiC MMCs reinforced with nano-sized particles (0.2 μm diameter). *Source* [29], with permission from Elsevier

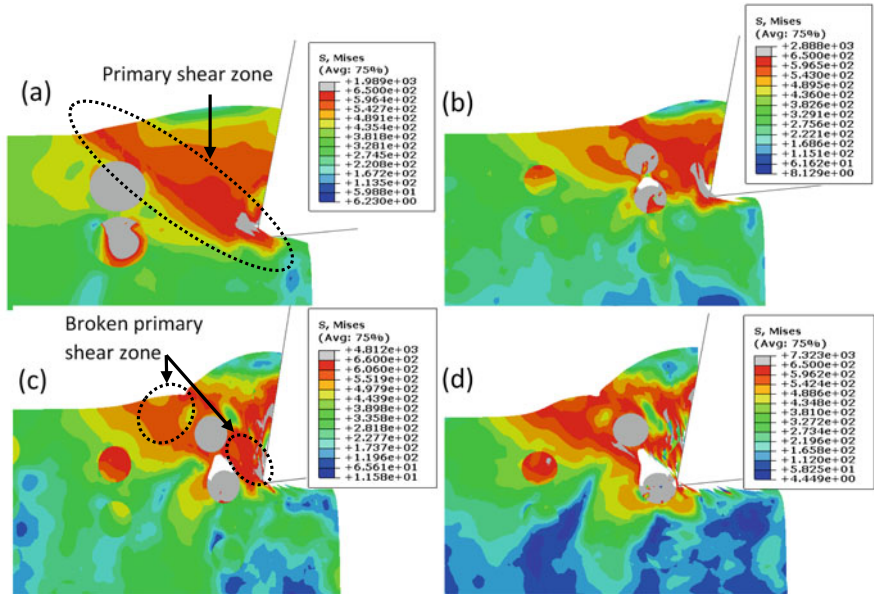

Fig. 19 Chip formation when micromachining of Al/SiC MMCs reinforced with micro-sized particles (10 μm diameter). *Source* [29], with permission from Elsevier

zone bear the greatest stress at both models. It proves the fact that hard SiC particles carry most of the load transferred from matrix materials. This can be attributed to the high elasticity of SiC particles. A different phenomenon in terms of von Mises stress distribution pattern within the matrix can be found between these two models when machining nano-MMCs (Fig. 18a), a narrow straight primary shear zone can be commonly found in machining homogeneous materials is not apparent. Instead, an irregular, highly concentrated stress zone was observed in the tool-workpiece interface, and the stress from the tooltip progresses to the upper surface with decreasing magnitude. With the cutting tool advances (Fig. 18b and c), a larger primary shear zone, when compared to that in machining homogeneous matrix materials (Fig. 20), becomes evident. In contrast, the primary shear zone can be observed when the cutting tool firstly engages with the workpiece and lasts during chip formation process in the model of machining micro-MMCs (Fig. 19a). The difference in the von Mises stress distribution between the two models implies that particles' location and size play a significant role in determining the stress propagation mechanism with the cutting tool's advancement.

In the model of machining nano-MMCs, a significant reduction in particle size tends to increase the number of particles involved in the machining area (uncut chip thickness) when compared to that in the machining of micro-MMCs. Unlike the highly concentrated stress region confined to the narrow primary shear zone in machining homogeneous materials (Fig. 20), these particles acting as barriers restrict

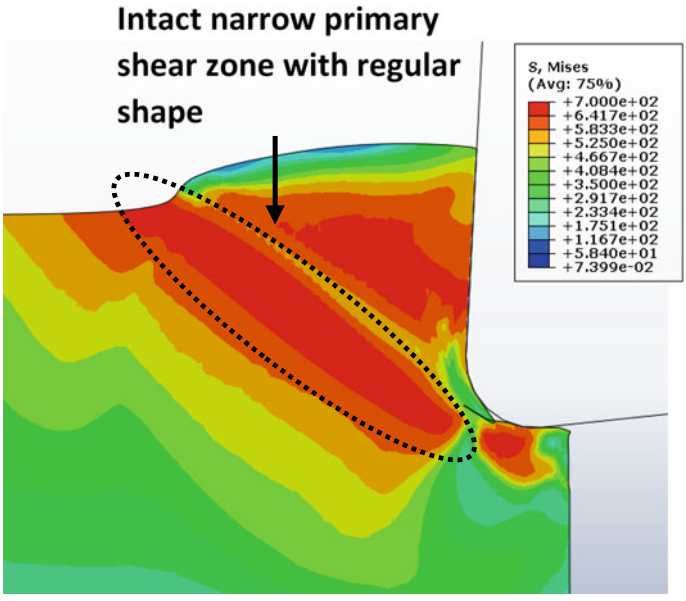

Fig. 20 Von Mises stress contour in machining pure Aluminium using the same cutting parameters of nano Al/SiC MMCs machining. *Source* [29], with permission from Elsevier

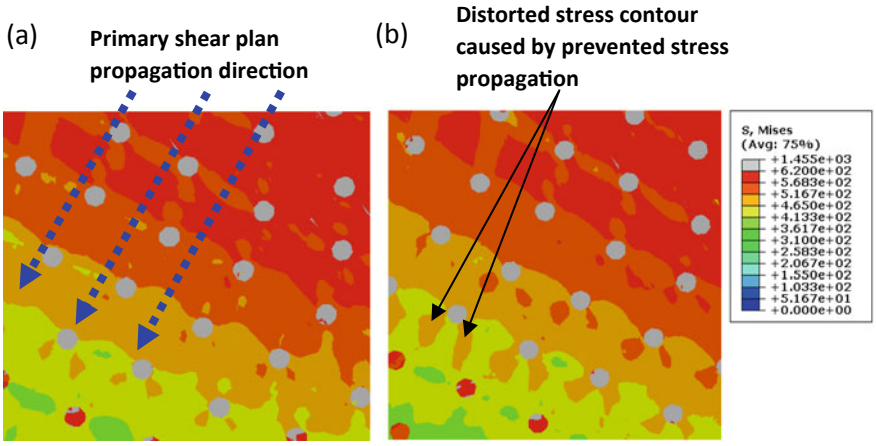

Fig. 21 Effect of nanoparticles on primary shear zone propagation **a** primary shear zone propagation direction; **b** distorted stress contour caused by prevented stress propagation. *Source* [29], with permission from Elsevier

the propagation of stress and force the highly concentrated stress to propagate to the surrounding area. This is believed to be the main reason leading to an irregular stress zone at the tool-workpiece interface at the initial cutting stage and larger shear zone with the cutting tool's advancement. A detailed study on restricting nanoparticles' behaviour is conducted by observing the primary shear zone propagation, as shown in Fig. 21. With the propagation of the primary shear plane, higher magnitude stress attempts to bypass the nanoparticle, which causes the irregular stress contour at the interface of each particle. As a result, a fragmented plastic strain field within matrix materials is formed due to the matrix's ability to deform plastically and particles' inability, see Fig. 22. The stress is therefore accumulated near the interface of particles and causes the highly concentrated plastic strain filed.

When the ratio between the particle diameter to uncut chip thickness increases, the particle's effect on stress distribution would be more dominant than that in nano-MMCs. By observing the von Mises stress pattern in the model of machining micro-MMCs, a significant difference when compared to that in machining nano-MMCs is that the particle size becomes comparable with the width of the primary shear zone (Fig. 19b–d). Similarly, micro-sized particles act as a barrier restricting the propagation of the primary shear zone. However, the primary shear zone is broken into two regions with a similar particle area and thus spread to surrounding when it is bypassing the micro-sized particle. Thus, greater compressive stress is generated on the particles under the squeezing action of cutting tool and matrix, resulting in a concentrated stress zone and maximum plastic strain on the tool-particle interface as shown in Fig. 23.

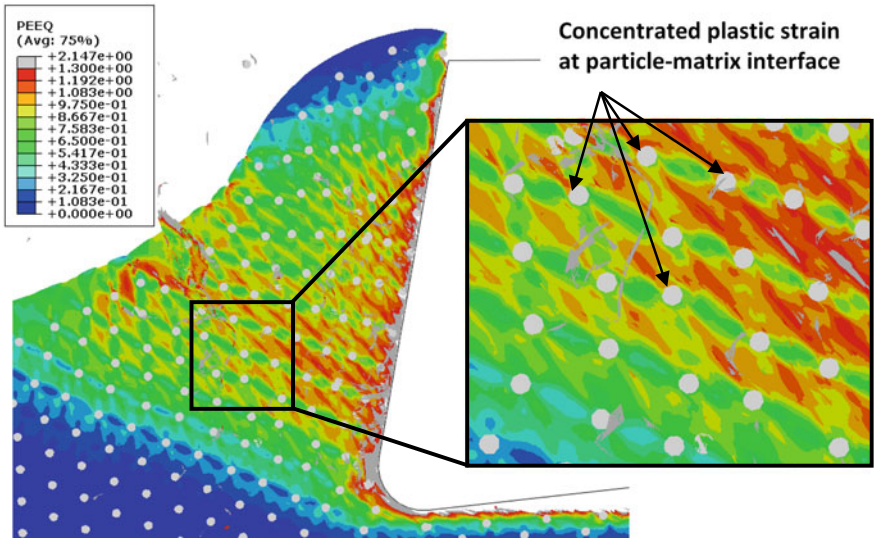

Fig. 22 Distorted plastic strain field in machining nano Al/SiC MMCs. *Source* [29], with permission from Elsevier

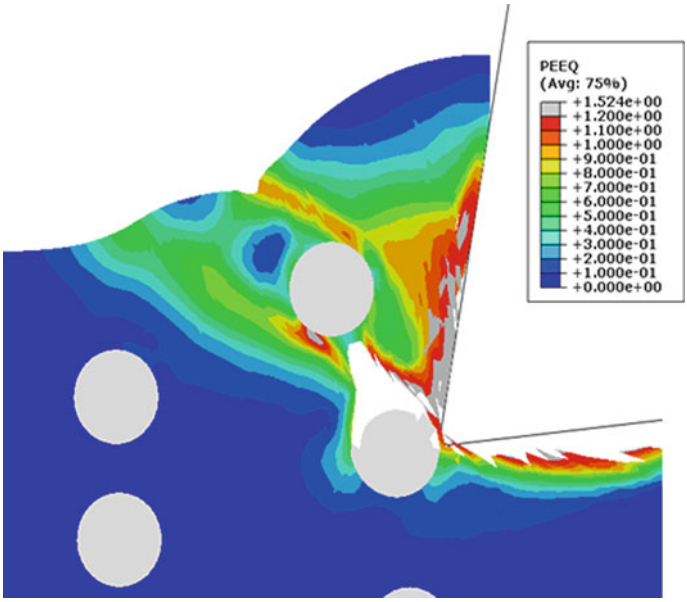

Fig. 23 Distribution of plastic strain filed in the machining of micro Al/SiC MMCs. *Source* [29], with permission from Elsevier

5.2 Tool-Particles Interaction

It is believed that the significant reduction in particle diameter from micro to nanoscale influence not only the stress distribution but also the tool-particle interaction. Figures 24 and 25 illustrate the tool-particle interaction in machining nano-MMCs and micro-MMCs, respectively. It can be observed from Fig. 24 that with the formation of a continuous chip, the particle embedded within formed chips slides over the rake face generating high localised stress at the tool-particle contact zone, which is similar as that for micro-MMCs. However, the nanoparticles are more likely to be squeezed by cutting edge due to their significantly large size difference, which leads to a relatively even distribution within particles. Also, the nanoparticles exhibit good mobility within the matrix, as mentioned earlier. As a result, nanoparticles keep intact without cleavage and fracture. In contrast, the micro-sized particles are observed to experience fracture.

Different behaviours of a particle interacting with the cutting tool in micro-MMCs machining process are shown in Fig. 25. It can be seen that the partially debonded particle is embedded within fragmented chips and slide along the cutting tool, resulting in the particle sliding behaviour on the tool rake face and a high localised contact region (Fig. 25a), which in turn would contribute to the tool wear. The particle located in the cutting path suffers a fracture. It was partially imbedded within the newly formed machined surface, which might be considered one of the main factors contributing to surface deterioration (Fig. 25b). Some particles located along or below the cutting path are pressed into the matrix (Fig. 19c). These particles acting as sharp cutting edge lead to the increased residual stress or severe plastic deformation on the machined surface. The particle detachment from the machined surface leading to the cavity can be observed from Fig. 25d. This phenomenon is

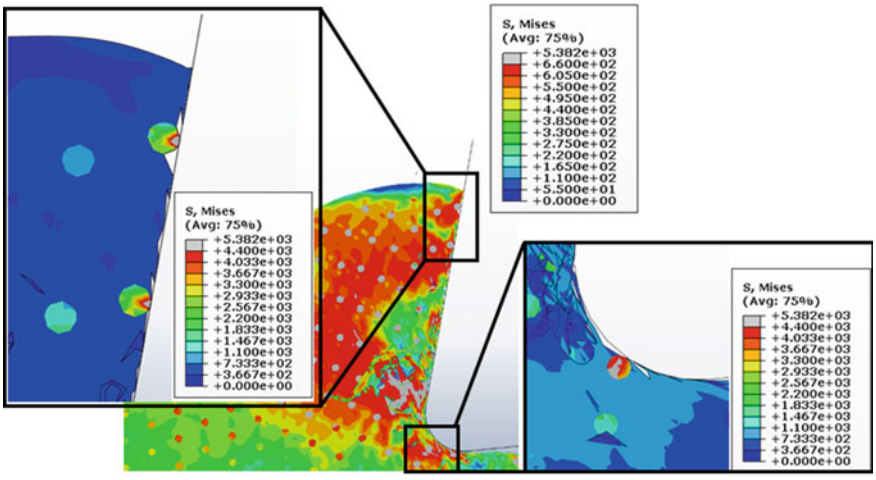

Fig. 24 Nanoparticles interacting with the cutting tool. *Source* [29], with permission from Elsevier

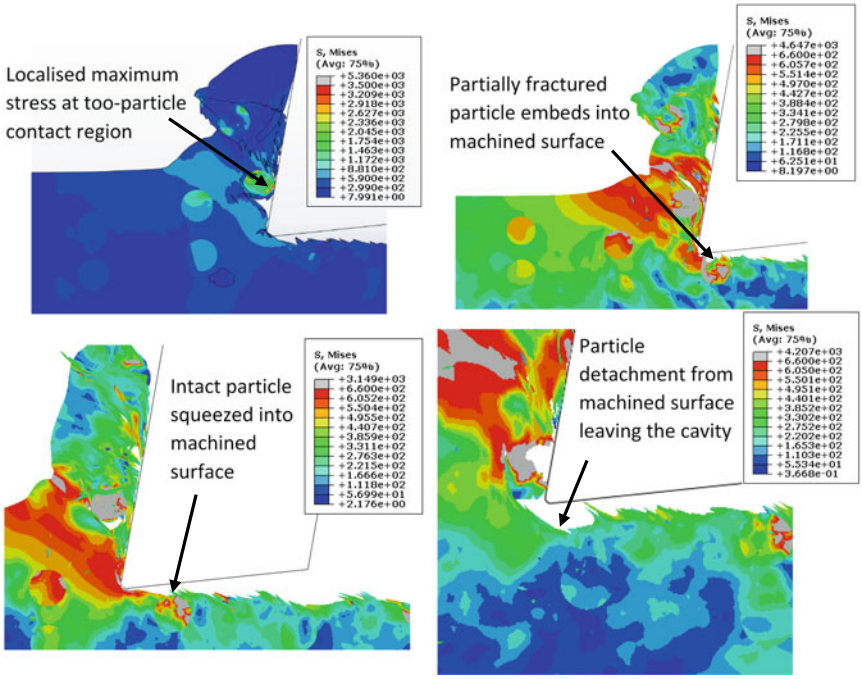

Fig. 25 Different tool-particle interaction behaviours in machining micro Al/SiC MMCs. *Source* [29], with permission from Elsevier

widely acknowledged by previous researchers in both experimental and simulation works.

The tool particle interaction can be visualised by analysing characteristics of the cutting force profile obtained from these two models (Fig. 26). Cutting forces from machining the homogeneous matrix material under the same cutting parameters are also plotted in Fig. 26. A larger cutting force fluctuation caused by the tool-particle interaction and fragmented chip formation is observed in the micro-MMCs machining process compared to homogeneous matrix materials. By comparison, apparent instability in cutting force obtained from machining nano-MMCs cannot be observed compared to that in machining homogeneous matrix. The larger cutting force fluctuation in machining micro-MMCs can be explained as results of various tool-particle interaction behaviours and the large particles' increased kinetic energy.

Generally, the tool-particle interface's high contact stress has been recognised as the main reason causing the tool wear. Various tool wear patterns can be obtained from machining nano and micro-MMCs, as shown in Fig. 27. Tooltip rounding and relatively smooth abrasive wear can be observed on the micro endmill's flank face in machining nano-MMCs (Fig. 27b). This can be attributed to the relatively small size of nanoparticles resulting in small kinematic energy compared to micro-sized particles during tool-particle interaction. Besides, good mobility of nanoparticles

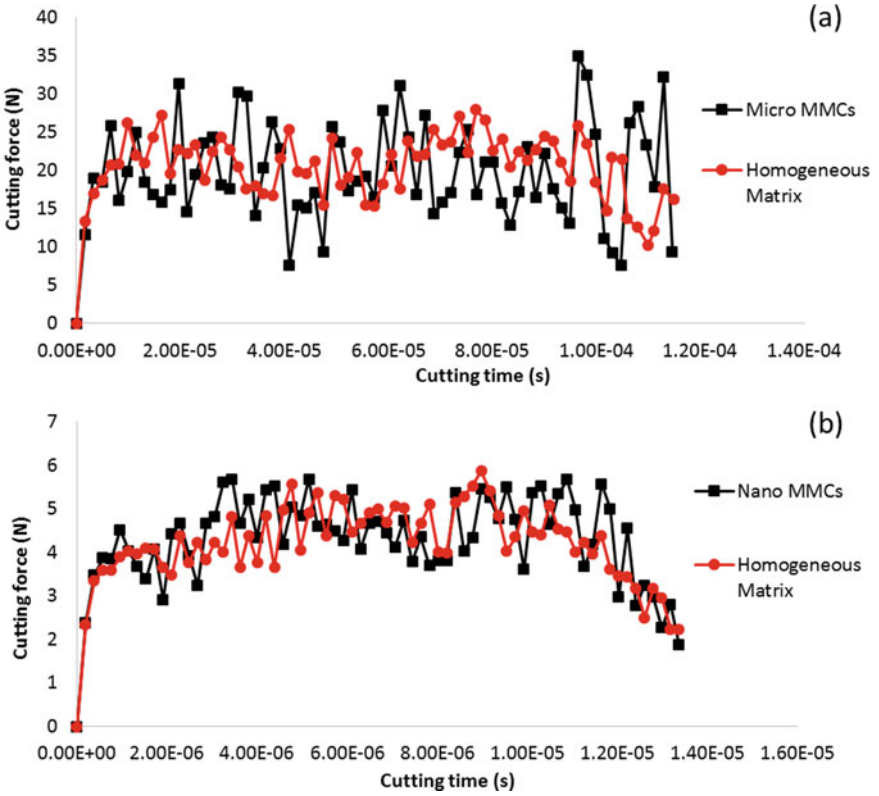

Fig. 26 Simulated cutting forces of micromachining Al/SiC MMCs reinforced with **a** micro-sized particles; **b** Nanoparticles. *Source* [29], with permission from Elsevier

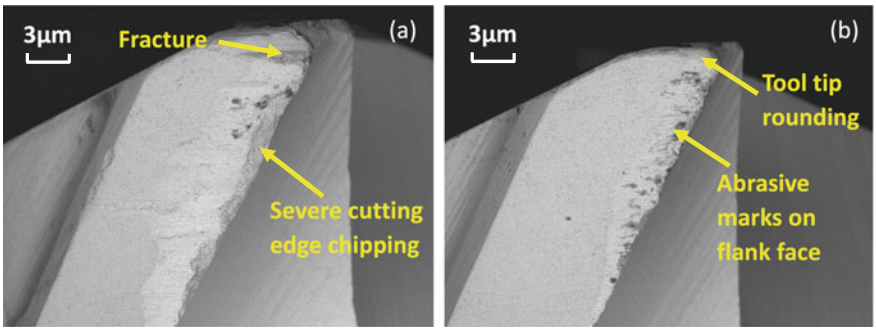

Fig. 27 SEM micrographs of main cutting edge wear of micro endmill obtained from machining Al/SiC MMCs reinforced with Vol. 10% **a** micro-sized particles (Φ:10 µm); **b** Nano-sized particles (Φ:0.2 µm) under feed per tooth of 4 µm/tooth, cutting speed of 125.64 m/min and depth of cut of 30 µm. *Source* [29], with permission from Elsevier

with matrix deformation is another crucial factor contributing to the smooth abrasive wear pattern. However, the low mobility of micro-sized particles within matrix materials and increased kinetic energy of micro-sized particles are believed to be the main reason that leads to a more severe edge chipping and fracture of tooltip on the endmill used in machining micro-sized MMCs, see Fig. 27a. Moreover, the unstable and fluctuating nature of the machining process caused by different tool-particles interaction behaviours accelerates the wear process.

5.3 Chip Formation Process

To analyse the chip morphology characteristics in machining the two MMC materials, it is necessary to understand the matrix's stress distribution. The size and location of particles play a significant role in the stress distribution pattern in the machining process. Figure 28 demonstrates the fragmented chips formation with stress distribution immediately after the chip formation shown in Fig. 19. Initially, the particles along the cutting path partially deboned without any direct contact with a tooltip, see Fig. 19b. With the tool advances, bypassing the primary shear plane occurred due to restricting the particle initiation behaviour. A highly concentrated stress zone is formed between the particle interface and upper surface of the workpiece in the shear plane and leads to crack initiation in the matrix, as shown in Fig. 28a. This crack initiation can be further proved by observing the high plastic strain field near this particle in Fig. 24. The plastic deformation mainly governs the MMCs workpiece behaviour in machining. As the tool advances, the matrix crack propagates towards the upper workpiece surface, as shown in Fig. 28b. Figure 28c shows the fragmented chips form.

Chips were collected from micro and nano-MMCs machining experiments to validate the chip formation models. The increased discontinuity can be observed at the sawtooth structure of the chips obtained from the machining of micro-MMCs (Fig. 29a). In contrast, continuous chips with saw tooth structure were found in machining nano-MMCs, as shown in Fig. 29b. The same observation was obtained from the experimental work conducted by Teng et al. [13]. It should be noted that although fragmented chips are formed in 2D FE simulation because the axial depth

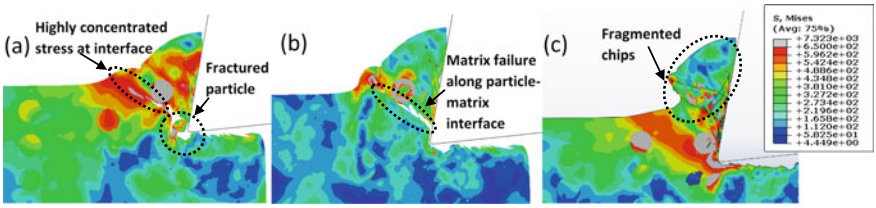

Fig. 28 Fragmented chips formation when micromachining of micro Al/SiC MMCs. *Source* [29], with permission from Elsevier

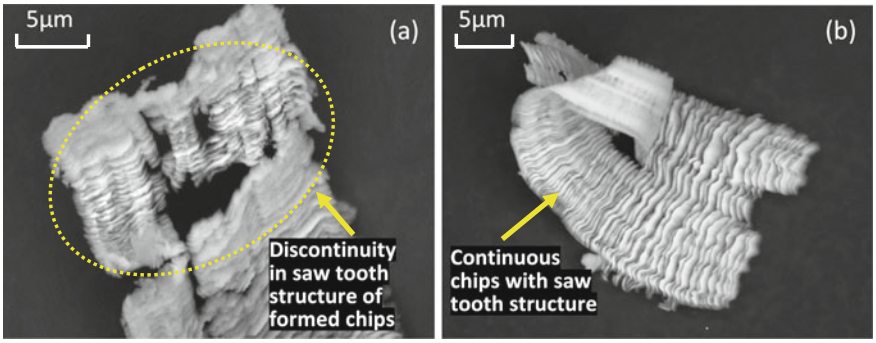

Fig. 29 SEM images of chips obtained from machining Al/SiC MMCs reinforced with Vol. 10% **a** micro-sized particles (Φ:10 μm); **b** Nano-sized particles (Φ:0.2 μm) under feed per tooth of 4 μm/tooth, cutting speed of 125.64 m/min and depth of cut of 30 μm. *Source* [29], with permission from Elsevier

of cut in the milling experiment is much greater than the micro-sized particle and also the micro-sized particles are randomly distributed in the matrix, the actual chips may not break along the width of the chip. Therefore, when observing a crossed section of the actual chips, the simulated chips morphology of micro and nano-MMCs shows high consistency with experimental results.

The highly concentrated stress zone can also be found at the particle–matrix interface in both models, as mentioned earlier. Therefore, it might not be the main reason for fragmented chips in the micro-MMCs machining process. The chip formation mechanism in machining micro-MMCs is depended on the size and location of particles which is the main factor determining the way of stress propagation. By comparing the width of the primary shear zone with particle size in these two models, it can be found that the shear zone is keeping intact during chip formation process in nano-MMCs rather than being fragmented in micro-MMCs. The existence of nanoparticle only affect the stress distribution pattern, and it does not significantly affect the overall integrity of the primary shear zone during its propagation. In other words, the restricting behaviour of micro-sized particles is more dominant than that in nanoparticles, which results in low mobility of particles within matrix deformation. This might be due to the sizeable uncut chip thickness to particle diameter in machining nano-MMCs. It can be thought that the location of nanoparticles has little effect on the chip formation mechanism in the nano-MMCs machining process. Therefore, the ratio of uncut chip thickness to particle size might be considered the fundamental reason was determining the chip formation mechanism. Finally, the intact primary shear zone means that the material removal is achieved by shear sliding in the nano-MMCs machining process. For micro-MMCs, as the result of strong restricting behaviour of micro-sized particles, the particle detachment from matrix caused by highly concentrated stress at its interface can be recognised as one factor promoting the formation of fragmented chips.

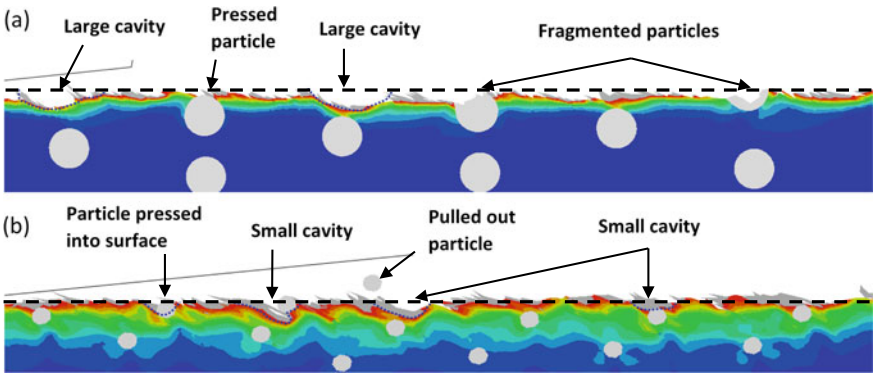

Fig. 30 Simulated surface morphology from machining **a** micro-MMCs; **b** Nano-MMCs. *Source* [29], with permission from Elsevier

5.4 Machined Surface Morphology

Different tool-particles interaction behaviours can be found in machining nano and micro-MMCs, leading to different machined surface morphology. Figure 30 shows the simulated surface morphology in machining micro and nano-MMCs. The surface deterioration in machining micro-MMCs can be attributed to the surface defects such as cavities, scratch marks, fragmented particles embedded within matrix and particles pressed into matrix causing excessive strain, which leads to a matrix failure (Fig. 30a). The abovementioned phenomenon obtained from simulation model can be easily observed from experimental results. It can be observed from Fig. 31a and b that the large cavity is formed when the majority of particles located in the cutting path are pulled away from the matrix during tool-particle interaction. Also, the fragmented particle embedded within the matrix is observed in Fig. 31a, consistent with simulated results. Excessive compressive stress would be caused by the particles pressed into the machined surface leading to the matrix failure or irreversible plastic deformation.

Moreover, during the cutting process, scratch marks on the machined surface will be formed when the fragmented particles act as sharp cutting edge being ploughed through between the flank face of the cutting tool and matrix. The magnified images of scratch marks marked in region i and ii can be found in Fig. 31b. Similar surface morphology can be observed in the simulation model of machining nano-MMCs (Fig. 30b). However, they are not observed in machined surface obtained from experimental works. Distinct milling tool path can be observed on the machined surface (Fig. 31c). Micro defects can be found at the tool path which broke its continuity. This might be caused by the scratching of residual chips containing nanoparticles at the tool-matrix interface during high-speed machining. It can be said that the significant reduction in particles size is beneficial for improving the machined surface quality.

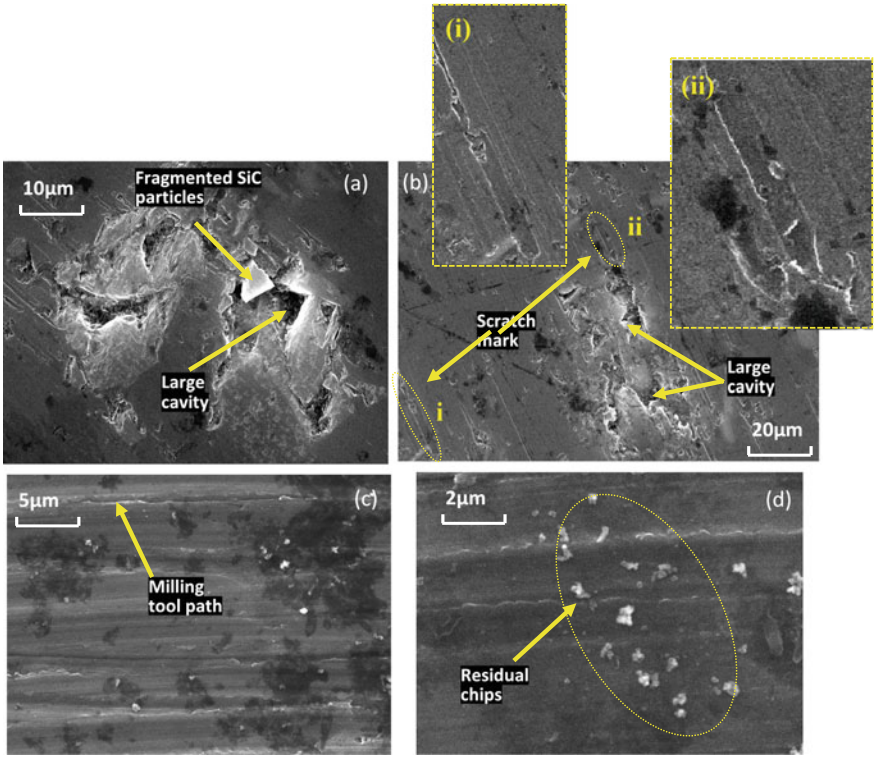

Fig. 31 SEM micrographs of the machined surface from experimental works **a** and **b** micro-MMCs; **c** and **d** nano-MMCs under the feed per tooth of 4 μm/tooth, cutting speed of 125.64 m/min and depth of cut of 30 μm. *Source* [29], with permission from Elsevier

6 Review Questions

(1) Please state the differences between macro-mechanical and micro-mechanical models.
(2) What are the primary materials removal mechanism revealed by the finite element modelling method when machining particulate MMCs?
(3) According to the simulation results, how do the reduced particles from micro-sized to nano-sized affect machinability? How do these relate to the results obtained from machining experiments?
(4) Please state the chip formation process of nano MMCs.
(5) Why do the particles near the primary shear zone take more stress than matrix materials?
(6) Please explain what can cause the distorted stress contour located at the vicinity of nanoparticles in FE analysis.
(7) Why would the addition of particle accelerate the progression of tool wear?
(8) What causes the lamellate structure of chips?

(9) How does the ratio of particle to uncut chip thickness affect the stress distribution during machining process?
(10) Please give the different behaviours of particles interacting with cutting tool in the machining process of micro MMCs.
(11) Please give the main types of surface defects in machining micro and nano MMCs and explain the reasons.
(12) How does the size effect affect the specific cutting energy?
(13) What causes different tool wear patterns when machining micro and nano MMCs?

References

1. Dandekar, C.R., Shin, Y.C.: Modeling of machining of composite materials: A review. Int. J. Mach. Tools Manuf. **57**, 102–121 (2012)
2. Monaghan, J., Brazil, D.: Modeling the sub-surface damage associated with the machining of a particle reinforced MMC. Comput. Mater. Sci. **9**(1–2), 99–107 (1997)
3. Monaghan, J., Brazil, D.: Modelling the flow processes of a particle reinforced metal matrix composite during machining. Compos. Part a Appl. Sci. Manuf. **29**(1–2), 87–99 (1998)
4. Pramanik, A., Zhang, L.C., Arsecularatne, J.A.: An FEM investigation into the behavior of metal matrix composites: Tool-particle interaction during orthogonal cutting. Int. J. Mach. Tools Manuf. 47(10), 1497–1506 (2007)
5. Zhu, Y., Kishawy, H.A.: Influence of alumina particles on the mechanics of machining metal matrix composites (tie constrains). Int. J. Mach. Tools Manuf. **45**(4–5), 389–398 (2005)
6. Dandekar, C.R., Shin, Y.C.: Multi-step 3-D finite element modeling of subsurface damage in machining particulate reinforced metal matrix composites. Compos. Part Appl. Sci. Manuf. **40**(8), 1231–1239 (2009)
7. Zhou, L., Huang, S.T., Wang, D., Yu, X.L.: Finite element and experimental studies of the cutting process of SiCp/Al composites with PCD tools. Int. J. Adv. Manuf. Technol. **52**(5–8), 619–626 (2011)
8. Zhou, L., Wang, Y., Ma, Z.Y., Yu, X.L.: Finite element and experimental studies of the formation mechanism of edge defects during machining of SiCp/Al composites. Int. J. Mach. Tools Manuf. **84**, 9–16 (2014)
9. Wang, B., Xie, L., Chen, X., Wang, X.: The milling simulation and experimental research on high volume fraction of SiCp/Al. Int. J. Adv. Manuf. Technol. **82**(5–8), 809–816 (2016)
10. Umer, U., Ashfaq, M., Qudeiri, J.A., Hussein, H.M.A., Danish, S.N., Al-Ahmari, A.R.: Modeling machining of particle-reinforced aluminum-based metal matrix composites using cohesive zone elements. Int. J. Adv. Manuf. Technol. **78**(5–8), 1171–1179 (2015)
11. Ghandehariun, A., Kishawy, H.A., Umer, U., Hussein, H.M.: Analysis of tool-particle interactions during cutting process of metal matrix composites. Int. J. Adv. Manuf. Technol. **82**(1–4), 143–152 (2016)
12. Ghandehariun, A., Kishawy, H.A., Umer, U., Hussein, H.M.: On tool-workpiece interactions during machining metal matrix composites: investigation of the effect of cutting speed. Int. J. Adv. Manuf. Technol. **84**(9–12), 2423–2435 (2016)
13. Teng, X., Huo, D., Chen, W., Wong, E., Zheng, L., Shyha, I.: Finite element modelling on cutting mechanism of nano Mg/SiC metal matrix composites considering cutting edge radius. J. Manuf. Process. 32 (2018)
14. Johnson, G., Cook, W.: A constitutive model and data for metals subjected to large strains, high strain rates and high temperatures. In: Proceedings of the 7th International Symposium on Ballistic, pp. 541–547 (1983)

15. Zerilli, F.J., Armstrong, R.W.: Dislocation-mechanics-based constitutive relations for material dynamics calculations. J. Appl. Phys. **61**(5), 1816 (1987)
16. Follansbee, P.S., Gray, G.T.: An analysis of the low temperature, low and high strain-rate deformation of Ti−6Al−4V. Metall. Trans. A **20**(5), 863–874 (1989)
17. Nemat-Nasser, S., Guo, W.-G., Nesterenko, V.F., Indrakanti, S.S., Gu, Y.-B.: Dynamic response of conventional and hot isostatically pressed Ti–6Al–4V alloys: experiments and modeling. Mech. Mater. **33**(8), 425–439 (2001)
18. Shi, J., Liu, C.R.: On predicting chip morphology and phase transformation in hard machining. Int. J. Adv. Manuf. Technol. **27**(7–8), 645–654 (2006)
19. Simoneau, A., Ng, E., Elbestawi, M.A.: Chip formation during microscale cutting of a medium carbon steel. Int. J. Mach. Tools Manuf. **46**(5), 467–481 (2006)
20. Abaqus/Explicit V6.14 User manual (2016)
21. Aurich, J.C., Bil, H.: 3D Finite Element Modelling of Segmented Chip Formation. CIRP Ann. Manuf. Technol. **55**(1), 47–50 (2006)
22. Ceretti, E., Lucchi, M., Altan, T.: FEM simulation of orthogonal cutting: serrated chip formation. J. Mater. Process. Technol. **95**(1), 17–26 (1999)
23. Hua, J., Shivpuri, R.: Influence of crack mechanics on the chip segmentation in the machining of Ti-6Al-4. In: Proceedings of the 9th ISPE International Conference on Concurrent Engineering, pp. 357–365 (2002)
24. Hillerborg, A., Modéer, M., Petersson, P.-E.: Analysis of crack formation and crack growth in concrete by means of fracture mechanics and finite elements. Cem. Concr. Res. **6**(6), 773–781 (1976)
25. Maekawa, K., Obikawa, T., Yamane, Y., Childs, T.H.C.: Metal Machining: Theory and Applications. Wiley, New York (2000)
26. Lai, X., Li, H., Li, C., Lin, Z., Ni, J.: Modelling and analysis of micro scale milling considering size effect, micro cutter edge radius and minimum chip thickness. Int. J. Mach. Tools Manuf. **48**(1), 1–14 (2008)
27. Liu, X., Devor, R.E., Kapoor, S.G., Ehmann, K.F.: The mechanics of machining at the microscale: assessment of the current state of the science. J. Manuf. Sci. Eng. **126**(4), 666–678 (2004)
28. Teng, X., Huo, D., Wong, E., Meenashisundaram, G., Gupta, M.: Micro-machinability of nanoparticle-reinforced Mg-based MMCs: an experimental investigation. Int. J. Adv. Manuf. Technol. 1–14 (2016)
29. Teng, X., Chen, W., Huo, D., Shyha, I., Lin, C.: Comparison of cutting mechanism when machining micro and nanoparticles reinforced SiC/Al metal matrix composites. Compos. Struct. **203**(July), 636–647 (2018)